

**ANALYSIS OF THREADED FASTENERS OF A HIGH STRENGTH STEEL:
ROLE OF FLAW SIZE AND ORIENTATION - A NUMERICAL STUDY**

CLAYTON REAKES, XIAOSHENG GAO AND T. S. SRIVATSAN

Department of Mechanical Engineering

The University of Akron / Ohio Polytechnic University

Akron, Ohio 44325-3903, USA

E-Mail (i) xgao@uakron.edu, (ii) tsrivatsan@uakron.edu

Abstract. This paper presents an investigation of the application of the technique of fracture mechanics to geometry of threaded fasteners. The flaw chosen is in the form of a surface crack and values of the J-integral along the crack front were evaluated using the computational technique. Variation in angular orientation of the crack, so as to simulate loading conditions similar to mixed mode I, II and III, was found to have an appreciable influence on overall value of the J-integral and stress state at the crack front. In this paper, the influence of variation in crack, or flaw, size on response kinetics of a threaded fastener was systematically investigated only to reveal an observable influence of flaw size on performance of the threaded faster made from high strength steel.

Keywords: threaded fasteners, cracks, crack or flaw size, fracture mechanics, finite element analysis, J-integral.

Introduction

Threaded fasteners have traditionally been one of the most commonly used components across all disciplines of engineering with specific reference to both structural and mechanical applications. A simple google search on failure of mechanical fasteners brings up several interesting case studies [1-6] wherein the structures failed as a direct consequence of fracture of the key fastener components. Despite sustained research and development efforts to both design and manufacture a flawless component, flaws (referred to henceforth through this manuscript as cracks) will inevitably make their way into mechanical components through the conjoint and mutually interactive influences of structure-material-environment interactions, such as corrosion [to specifically include: (i) embrittlement by hydrogen, and (ii) stress corrosion cracking]. This has provided the much needed interest to examine fracture properties of geometry of a fastener with an emphasis on using the technique of non-linear fracture mechanics.

The usefulness of stress intensity factor (K)-dominated methods [7] outside of linear elastic conditions, is highly limited [8]. With an increased emphasis on nonlinear dominance of the stress state, a method implementing the use of path-independent J-integral [9] did eventually become essential. This will help in defining the deformation state of the crack.

1. The J-Integral

A two-dimensional analysis of the path independent J-integral initiates by examining a non-linear elastic homogeneous body that is essentially: (i) free of all body forces, and (ii) acted on by a two-dimensional deformation field. The body is comprised of an elastic material that experiences a Hookean response within the yield surface with nonlinear hardening occurring immediately outside of the yield surface. Rice [9] defined the path independent J-integral to be:

$$J = \int_{\Gamma^*} \left(W dy - \mathbf{T} \cdot \frac{\partial \mathbf{u}}{\partial x} ds \right) \quad (1)$$

where W is the strain energy density, \mathbf{T} is the traction vector and \mathbf{u} is the displacement vector. Describing the contour path in a fashion that results in the integral of $W dy - \mathbf{T} \cdot \frac{\partial \mathbf{u}}{\partial x} ds$ vanishing, can be shown that the sum value of the integral along the counter-clockwise path is zero. This path independence is inferred to a path that gives the same value of J , given the area between the paths is free of singularities. With focus on an area immediately around the crack tip the J-integral becomes representative of the local field.

When developing a finite element model to determine the J-integral values for the Boundary-Layer model, it is important to have a method that helps in verifying the overall validity of the model and the calculations involved. This is performed by using the equations of small-scale yielding (SSY) developed and put forth by Rice [10]. In his analysis, Rice examined the case of a narrow crack in a body that was loaded to induce a yield zone both at and near the crack tip that, relative to its dimensions, is conceived as being noticeably small.

The formulation begins by means of defining polar coordinates (r, θ) for the boundary-layer problem with the origin located at the tip of the crack. This is shown in **Figure 1**. Assuming the plastic zone to form near the crack tip, in an elastic-perfectly plastic material for which the load level is sufficiently small, it can be assumed that singularity controls the stresses at a significant distance away from the crack tip. From this method, we get an equation for the stress state in the immediate vicinity of the crack tip as the radius (' r ') approaches infinity

The

$$\sigma_{ij} \rightarrow \frac{K_I}{(2\pi r)^{\frac{1}{2}}} f_{ij}(\theta) \quad \text{as } r \rightarrow \infty \quad (2)$$

J-integral is formulated using the boundary layer solution parameters, taking the contour (Γ) to be a large circle having a radius r . Allowing the radius (r) to approach infinity and noting the strain energy density to be quadratic in the strain region it was found that only the asymptotically approached inverse square-root elastic-stress field contributes to the J-integral analysis. Using the associated plane-strain deformation field we get:

$$J = \frac{1 - \nu^2}{E} K_I^2 \quad (3)$$

where E is young's modulus for the material, ν is Poisson's ratio and K_I is the Mode I stress intensity factor.

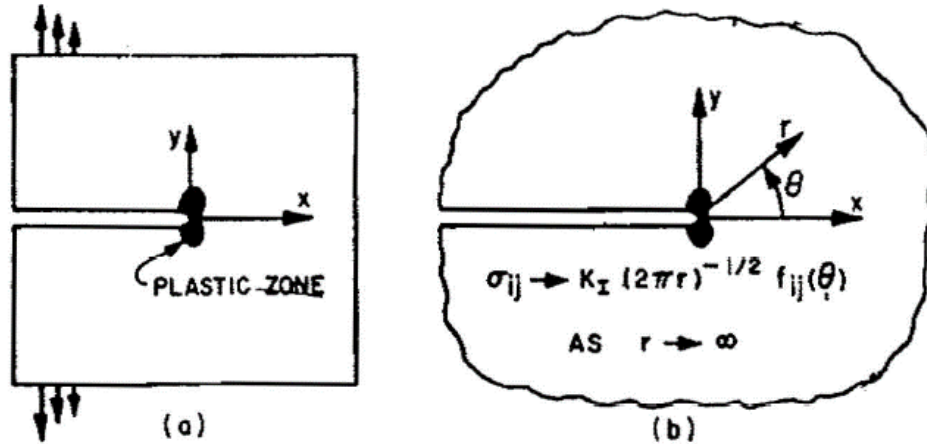


Figure 1. (a) Small-scale yielding example for a crack in an elastic plastic material with geometrically exact boundary conditions.

(b) Configuration of crack in a semi-infinite body in which the actual boundary conditions are replaced with an asymptotic method

Equation 3 provides a mathematical method for purpose of checking accuracy of the finite element boundary layer model by enabling calculation of the K value that can be associated with the output J -value. An agreement with the K value used to determine the displacement field values on the boundary layer does clearly indicate the finite element model to have sufficient contours for the purpose of achieving a path-independent state.

The Hutchinson-Rice-Rosengren (HRR) solution provides a viable method for showing the J -integral to characterize the crack-tip conditions for a non-linear elastic material [11, 12]. Uniaxial deformation, taking into account material that follows the power-law hardening and with the inclusion of elastic strains, can be defined using the Ramberg-Osgood equation:

$$\frac{\varepsilon}{\varepsilon_0} = \frac{\sigma}{\sigma_0} + \alpha \left(\frac{\sigma}{\sigma_0} \right)^n \quad (4)$$

In this expression, σ_0 is the reference stress, $\varepsilon_0 = \sigma_0/E$, α is a dimensionless material constant and 'n' is the strain-hardening exponent. It was shown that path independence can be maintained when stress-strain is varied using $1/r$ near the tip of a flaw or crack. Stress-strain relationships can be reduced to a power-law function at distances very close to the tip of a flaw or crack. At this location the elastic strains are noticeably small when compared to the total strain [13]. Application of boundary conditions provides an ability to obtain the stress-strain distribution using the following relationships:

$$\sigma_{ij} = \sigma_0 \left(\frac{EJ}{\alpha \sigma_0^2 I_n r} \right)^{\frac{1}{n+1}} \tilde{\sigma}_{ij}(n, \theta) \quad (5)$$

$$\varepsilon_{ij} = \frac{\alpha \sigma_0}{E} \left(\frac{EJ}{\alpha \sigma_0^2 I_n r} \right)^{\frac{n}{n+1}} \tilde{\varepsilon}_{ij}(n, \theta) \quad (6)$$

In these two equations: (i) I_n is an integration constant depending on n , (ii) σ_{ij} and ε_{ij} are dimensionless functions of n and θ . Equation 6 and Equation 7 are also known as the HRR singularity.

2. The Numerical Model and Approach

2.1. Material Definition

ABS Grade DH36 steel, a material for which the stress and strain information was readily available from Gao et al. [14, 15], is used in this research study. The chosen material, i.e., DH36 is a structural steel with high strength that offers a combination of enhanced corrosion resistance, good fracture toughness coupled with strong processing and adequate welding characteristics [16]. The Young's modulus of this material is 200GPa and the Poisson's ratio is 0.3. The stress-strain curve subsequent to plastic yielding was fit to a power-law hardening relationship in conformance with Equation 7 using $\sigma_0 = 345\text{MPa}$ and $n = 0.143$:

$$\varepsilon = \frac{\sigma_0}{E} \left(\frac{\sigma}{\sigma_0} \right)^{1/n} \quad (7)$$

In this equation E is the modulus of elasticity, σ_0 is the yield stress and 'n' is taken to be the strain hardening exponent. Although this investigation focuses solely on high strength structural steel DH36, additional tests can be conducted using the same fastener geometry for different high strength metals by simply changing the inputs to the stress-strain curve in the finite element program to conform to the chosen material.

2.2. Finite Element Model

Non-linear finite element analysis [FEA] was conducted using Simulia Abaqus / Standard [17] as the FEA pre-processing and post-processing tool. For the case of three-dimensional models all meshing was conducted using Hyperworks Hypermesh [18] and imported into Abaqus to facilitate for more intricate controlled modeling of events that exist immediately ahead of the chosen crack. Three-dimensional computer-aided design (CAD) modeling was performed using Autodesk Inventor [19].

2.3. The Plane Strain, Small-Scale Yielding model

For this investigation a Modified Boundary Layer (MBL) analysis was performed to develop a wide array of solutions for the zone at the crack tip. Solution to the modified boundary layer [MBL] helps simplify the analysis at the crack tip by using a set of equations for purpose of enforcing a far-field stress on the boundary layer so as to simulate response at the crack tip [10]. The plastic region is limited to a small portion of the far-field radius (R) and for a value of $R_p < R/20$ to ensure validity of the K-dominated zone as

definition of the boundary condition. Numerical solutions were obtained by imposing displacements on the far-field nodes for purely an elastic response under Mode I loading in the region ($r = R$)

$$u(R, \theta) = K \frac{1 + \nu}{E} \sqrt{\frac{R}{2\theta}} \cos\left(\frac{\theta}{2}\right) (3 - 4\nu - \cos(\theta)) + T \frac{1 - \nu^2}{E} R \cos(\theta) \quad (8)$$

$$v(R, \theta) = K \frac{1 + \nu}{E} \sqrt{\frac{R}{2\theta}} \sin\left(\frac{\theta}{2}\right) (3 - 4\nu - \cos(\theta)) + T \frac{-\nu(1 + \nu)}{E} R \sin(\theta) \quad (9)$$

To enhance convergence of the nonlinear iterations a small initial root radius at the tip of a crack was adopted. It was shown in earlier studies that the initial notch radius will have no effect on the numerical results once the crack-tip opening displacement (CTOD) becomes greater than four times the value of the initial radius [20,21]. In this study, the initial radius of the notch was taken to be $1.25\mu\text{m}$. This is shown in **Figure 2b**. The modified boundary layer (MBL) model was constructed using 2,771 two-dimensional quadratic eight-node iso-parametric plane-strain elements and having reduced integration elements so as to accurately capture the stress state in the J-Q annulus.

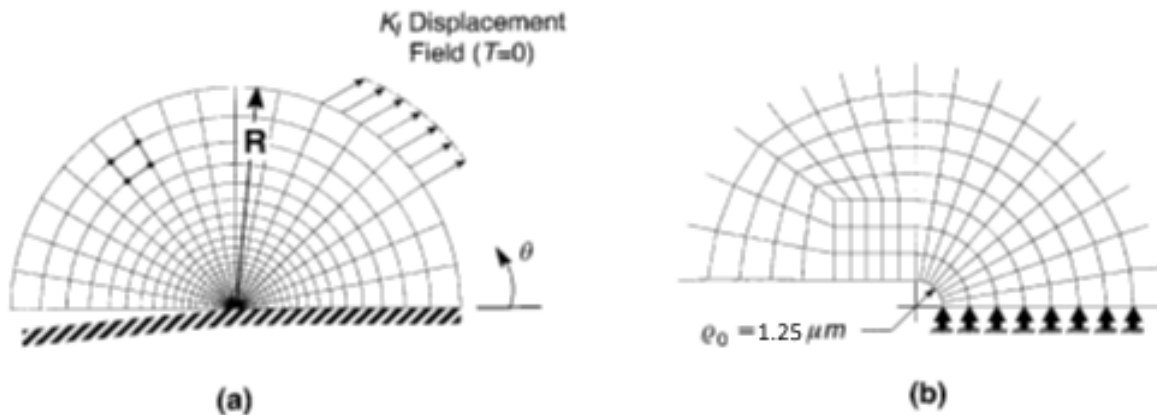


Figure 2. (a) For small-scale yielding (SSY) model with K_I displacement field and R - θ coordinate system.
(b) Near-tip mesh with initial root radius of $1.25\mu\text{m}$

2.4. The Finite Element Elliptical Flaw Fastener Model

To be studied is a 12.7mm-0.512 x 50.8mm (1/2in-13 x 2in) fully-threaded socket head cap screw. The three-dimensional [3D] CAD model shown in **Figure 3** provides an overview of geometry of the threaded fastener. A slice at the region of flaw, or crack, is shown in **Figure 4**. The model was adapted by cutting away material to account for the clip gage that is normally used in laboratory-scale tests. This was done by removing a section of thread having a length of 20.32mm to account for length of the gage and by cutting a notch having a size of 0.762mm for purpose of attaching the clip gage.

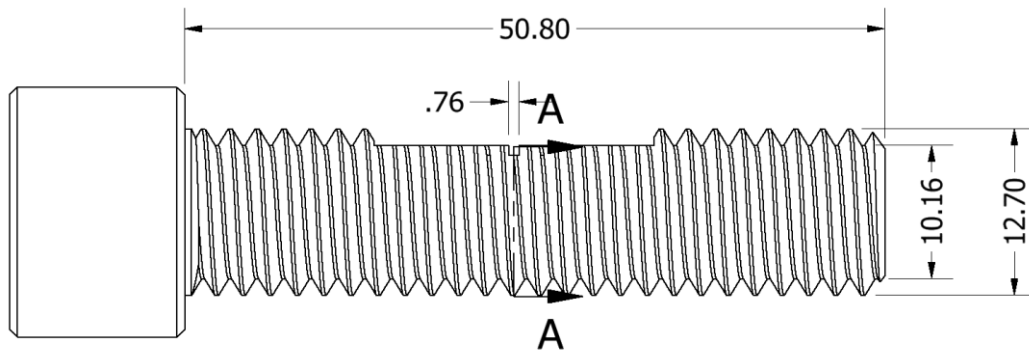


Figure 3. 12.7mm-13 x 50.8mm (1/2in-13 x 2in) fully threaded socket head cap screw with necessary modifications for clip gauge placement

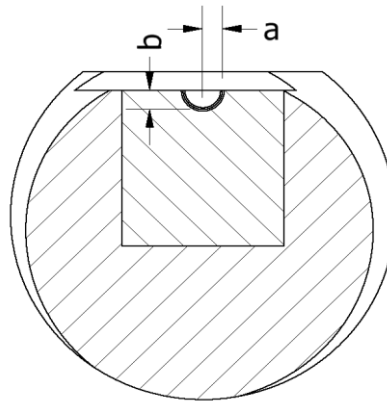


Figure 4. Configuration of the crack front for J-integral computations

Geometry of the crack was modeled as an elliptical crack having varying values of width [$2a$] and depth [b]. Elliptical shaped flaws were chosen for this study due to their occurrence as flaws present on the surface of most service components. A schematic showing key control variables of an elliptical crack is shown in **Figure 6**. The two-dimensional (2-D) crack mesh was extruded along an elliptical arc to create 30 layers of elements having equal spacing along length of the arc. This modeling method provided 31 regions for purpose of calculating the J-integral along with 40 contours in each region, which proved sufficient for purpose of ensuring path independence.

The crack tip is modeled as a small notch due to primary interest in results in the plastic range. A blunt crack tip helps in controlling distortion of the element resulting from incompressibility of the elastic-plastic material in the non-linear range. The crack-tip mesh along with views of the contour and global crack region are shown in **Figure 5**. A unit cell, containing the crack geometry, was used in conjunction with a pre-meshed model of the threaded fastener by enforcing a tie constraint on the contacting surfaces.

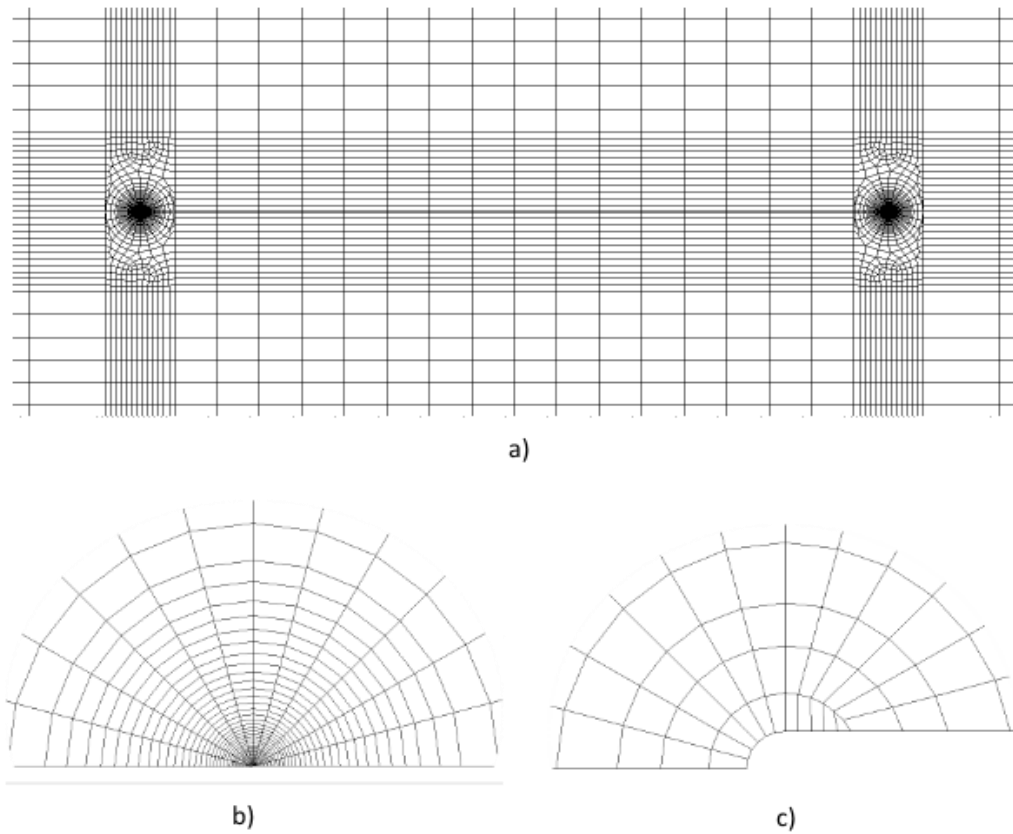


Figure 5. Mesh of three-dimensional model examined
 a) zoomed out view of crack front area
 b) contour mesh with external radius of 0.12mm, and
 c) near-field crack tip mesh with crack tip radius of 1.25μm

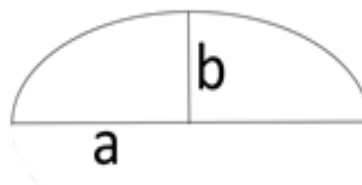


Figure 6. Definition of Control Variables for an Elliptical Crack.

The J-integral values were calculated using a domain integral method at each node set P along the crack front as defined by documentation manual of the ABAQUS version 6.13 [20].

$$J^P = \bar{J}^P / \int_L N^P ds \quad (10)$$

In this expression, J^P is the J-integral at node set P and N^P is a node set that is located at a value s along the crack front.

3. Numerical Results

3.1. Variation of the J integral value along a crack front

By examining the effects of a crack on values of the J integral, the models were evaluated at each contour region to obtain a plot of the J-integral value versus the ratio of crack length progressing from 0 to 1. The values of “s” were calculated numerically using an elliptical integral that was evaluated at the node points along the crack front. These values were subsequently divided by length of the largest arc so as verify that final value of the ratio was 1. The load level was selected by looking at the values of J that were expected at a node point that existed in the mesh. With a node located at a radial distance from the center point of a crack of length 3.07×10^{-3} mm, the equation $J = 2 \sqrt{r} \sigma_0$ was used to obtain a J value of 0.53 mJ/mm^2 . Due to an interest in investigating the crack at a value of $s=0.5$, **Figure 7** was plotted using a load step that provided a J value of 0.53 at the node associated with $s=0.5$.

Results obtained for the specimen having crack dimensions of $a=1.651\text{mm}$ and $b=1.651\text{mm}$, are shown in **Figure 8**. This figure reveals a strong correlation to exist between position along the crack front and expected value of the J integral. There does occur a peak in value of the J integral for values of $s=0.065$ and $s=0.935$, with an observable drop in the J integral value occurring on either side of this point. This is due to a loss in constraint that occurs near $s=0$ and $s=1$ coupled with an observable reduction in contribution of the bending stress as depth of the crack gradually increases towards the center line of loading. Values for this configuration peak to a J integral value of 0.84 mJ/mm^2 and bottom out at a J integral value of 0.530 mJ/mm^2 .

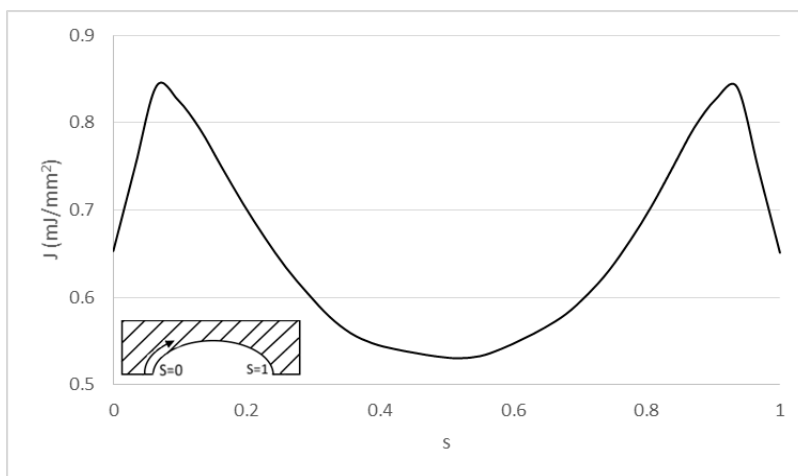


Figure 8. Variation of J along the crack front plotted against the ratio of arc length for a specimen with crack dimensions of $a=1.651\text{mm}$ and $b=1.651\text{mm}$ at a load of 5.5 kN.

3.2. Influence of Crack Aspect Ratio on J

The next step was to examine the effect changes in dimensions of an elliptical crack had on the value of the J integral across the crack front. For purpose of analysis, models having crack dimensions of (i) $a = 1.651\text{mm}$ $b = 1.651\text{mm}$, (ii) $a = 1.651\text{mm}$; $b = 2.54\text{mm}$, (iii) $a = 2.54\text{mm}$, $b = 1.651\text{mm}$, and (iv) $a = 2.54\text{mm}$, $b = 2.54\text{mm}$ were chosen so as to provide cases of variation in crack geometry for each configuration of the ellipse. All positional data was normalized along the crack front to give values of s from 0 to 1, and for all models the data was collected for a value of $s = 0.5$ and $J=0.53$. The results shown in **Figure 7** reveal the following: (a) increasing the depth of the crack tip does increase the value of the J-integral, and (b) increasing the width of the crack causes an observable decrease in the value of J.

From the results for $a = b = 2.54\text{mm}$ it is seen that the effect of increasing the depth of a crack had a greater influence on deformation state of the crack than increasing width of the crack. This is evident because a proportional increase in size causes an unproportioned shift in the curve. It is worth noting that values of the J integral for a flaw having dimensions of $a = 1.651\text{mm}$ and $b = 2.54\text{mm}$ were taken at both a lower value and higher value of the load due to a gap in the analysis intervals. The observed difference in values of the J integral along the crack front was found to be minimal and only the results for a value of the J integral that is lower than 0.53, at a location $s = 0.5$, is shown.

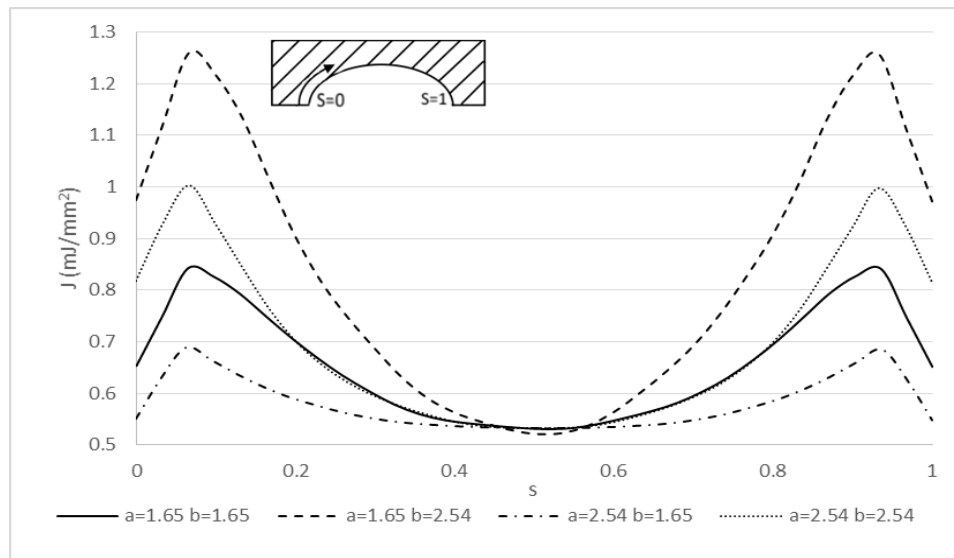


Figure 7. Values of J integral plotted against arc length ratio for multiple elliptical crack geometries

Seeing an obvious dominance on the state of J with changes in crack position it is of interest to show changes in value of the J integral at the root of a crack with changing crack aspect ratio. In **Figure 9** is shown the results for J integral at the root of a crack with

the value ‘ a ’ being held constant at 1.651mm and b being allowed to vary from 0.762mm to 3.429 mm for a selected crack-mouth opening displacement (CMOD) of 0.003mm. From these results a noticeable decrease in value of the J integral for ratios below 1/1 and a slight decrease in value of the J integral for ratios above 1/1 were observed. Value of the J integral at the crack root for same ratios of a/b was plotted for varying load steps and as shown in **Figure 9** for the following values of the CMOD: (i) 0.0015mm, (ii) 0.003mm, and (iii) 0.0045mm. From this figure it can be seen that the magnitude of loading had an appreciable influence on how the crack ratio manipulates value of the J integral at the root of a crack. For a high level of loading, a negative slope or decrease in value of the J integral beyond an aspect ratio of 1/1 gains magnitude resulting in a sharp decrease in value of the J integral. At low levels of loading, the slope of the J curve actually switches to a positive value, causing an increase in value of the J integral beyond a crack ratio of 1/1. Holding b constant and at 1.651mm while allowing a to vary from 0.762mm to 3.429mm a difference in behavior can be seen as shown in **Figure 10**, with an observable increase in the J integral value for a variance of a both below and above a ratio of 1/1. Slope of the J integral curve on either side of a 1/1 ratio does see the influence of loading with a noticeable increase in magnitude as the load increases. The value of J at the crack tip for the case of low loading does reach a near linear state.

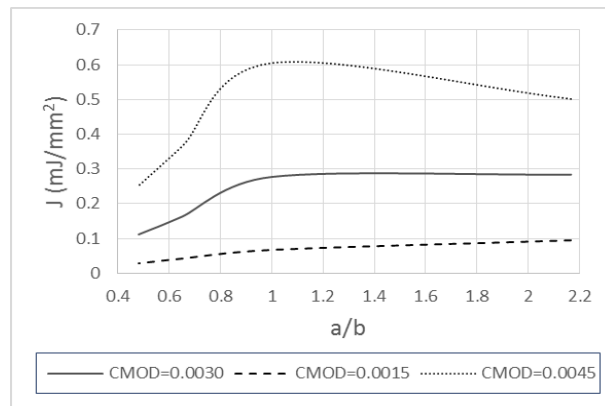


Figure 9. J integral value at $s=0.5$ plotted against crack aspect ratio (a/b) for multiple CMOD values of 0.0015mm, 0.0030mm and 0.0045mm.

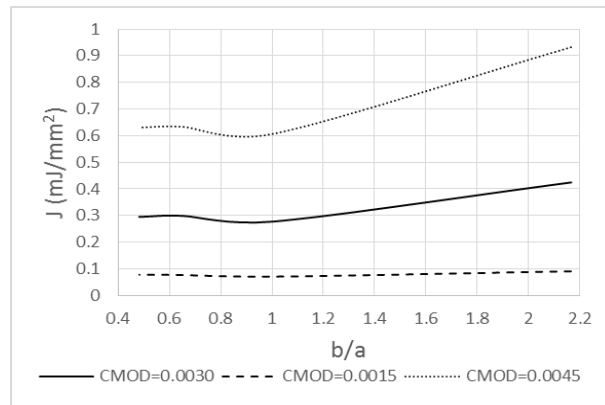


Figure 10. J integral value at $s=0.5$ plotted against crack aspect ratio (b/a) for multiple CMOD values of 0.0015mm, 0.0030mm and 0.0045mm

Table 1. Crack root J-integral data for models of varying crack size holding one geometric dimension as a constant and varying the secondary variable

Constant (mm)	CMOD (mm)	b(mm)	a/b	b/a	J (mJ/mm ²)
a=1.651	0.0015	0.762	2.167	0.462	0.095
		1.651	1.000	1.000	0.067
		2.540	0.650	1.538	0.042
		3.429	0.481	2.077	0.028
	0.003	0.762	2.167	0.462	0.284
		1.651	1.000	1.000	0.277
		2.540	0.650	1.538	0.163
		3.429	0.481	2.077	0.112
	0.0045	0.762	2.167	0.462	0.502
		1.651	1.000	1.000	0.605
		2.540	0.650	1.538	0.364
		3.429	0.481	2.077	0.252
Constant(mm)	CMOD (mm)	a (mm)	a/b	b/a	J (mJ/mm ²)
b=1.651	0.0015	0.762	0.462	2.167	0.092
		1.651	1.000	1.000	0.071
		2.540	1.538	0.650	0.077
		3.429	2.077	0.481	0.079
	0.0030	0.762	0.462	2.167	0.425
		1.651	1.000	1.000	0.277
		2.540	1.538	0.650	0.299
		3.429	2.077	0.481	0.295
	0.0045	0.762	0.462	2.167	0.934
		1.651	1.000	1.000	0.605
		2.540	1.538	0.650	0.633
		3.429	2.077	0.481	0.630

4.3 Changes to Angular Orientation of the Flaw or Crack

With an understanding of how changes in crack size can exert an influence on value of the J-integral at the crack front for a flaw, or crack, that is normal or perpendicular to direction of loading, an investigation was initiated into understanding the influence of

changes in orientation of the crack on value of the J integral as it deviates from a purely Mode I loading mode. For this investigation, a single model with a crack having the dimension of $a = b = 1.651\text{mm}$ and rotated by -10 degrees from the original crack plane was considered. This is shown in **Figure 11**. All other parameters for modeling were held constant to include the following: (i) elements along the crack front, and (ii) number of contours in the J-integral region of the model.



Figure 11. Visualization of crack tip rotated -10 degrees from the original crack plane.

Values of J integral along the crack contour (s) were plotted for a displacement value of 0.037mm for situations of both a and b having a value of 1.651 and the angle (θ) being equal to the following (i) 0 degrees, (ii) -10 degrees, and (iii) -30 degrees, as shown in **Figure 12**. The observed negative trend in value of the J integral is seen for all regions with noticeable increase in the magnitude of difference in the following regions: (1) $s=0.04$, (2) $s=0.22$, and (3) $s=0.5$ for the case of θ being equal to -10 degrees. However, for $\theta = -30$ degree the model reveals a large reduction in value of the J integral being equal across all regions with the decrease in magnitude being equal across the crack front. The numerical results reveal orientation of the crack to have a scaling effect on value of the J integral at the crack tip. Further, little difference was observed in those regions where loading was essentially perpendicular to the crack plane. Examining the curve for an orientation of the crack at -30 degrees, the effect and/or influence is observably significant. At this point, it is safe to conclude that loading on the crack front has shifted away from primarily Mode I to one in which contributions from Mode II and Mode III loading modes cannot be ignored.

The contributions from Mode II and Mode III loading play a much larger role on values of the J-integral at the crack tip. This is shown in **Figure 13**. In this figure, the values are taken at the same value of the J integral. A similar value of the J-integral at the root of a crack results in an actual decrease in value of the J integral along the crack front. For crack orientation angles of $\theta = -10$ degrees and $\theta = -30$ degrees, the results reveal a magnitude decrease in the value of the J integral along the contour (s) between $s = 0.07$ and $s = 0.15$. This change in slope provides a viable explanation for an initial increase in the value of the J integral with rotation of the crack with respect to the load axis and ultimately resulting in an observable decrease in value of the J-integral as the crack orientation angle increases.

Table 2. Tabular data showing the effects of crack orientation on J across the crack front of a crack with dimensions a=b=1.651

θ	Normalized position along crack front, s										
	0	0.1	0.2	0.3	0.4	0.5	0.6	0.7	0.8	0.9	1
	J (mJ/mm ²)										
0	0.409	0.473	0.384	0.318	0.286	0.277	0.286	0.316	0.380	0.471	0.406
-10	0.410	0.474	0.376	0.314	0.280	0.271	0.279	0.312	0.372	0.470	0.407
-30	0.330	0.407	0.328	0.272	0.245	0.240	0.244	0.270	0.325	0.403	0.327

Examining the influence change in orientation of the crack had on stress state of the chosen model, variation of the values of hydrostatic stress with orientation angle (θ) is plotted and is shown in **Figure 14**. Results reveal a change in orientation of the crack to cause a noticeable change in the hydrostatic stress state immediately ahead of the crack tip. To begin with, peak of the hydrostatic stress curve is shifted to the left with the magnitude remaining effectively the same. As the angle θ progresses into the negative zone, an observed decrease in the value of hydrostatic stress is seen. This decrease is attributed to the conjoint influence of decrease in both bending stress and tension stress in this region. For a θ value of 180 degrees, the hydrostatic stress state of the angled crack reveals a significant increase in comparison with the flat crack. This occurs because stresses in this region increase as the crack begins to align itself with the plane of loading.

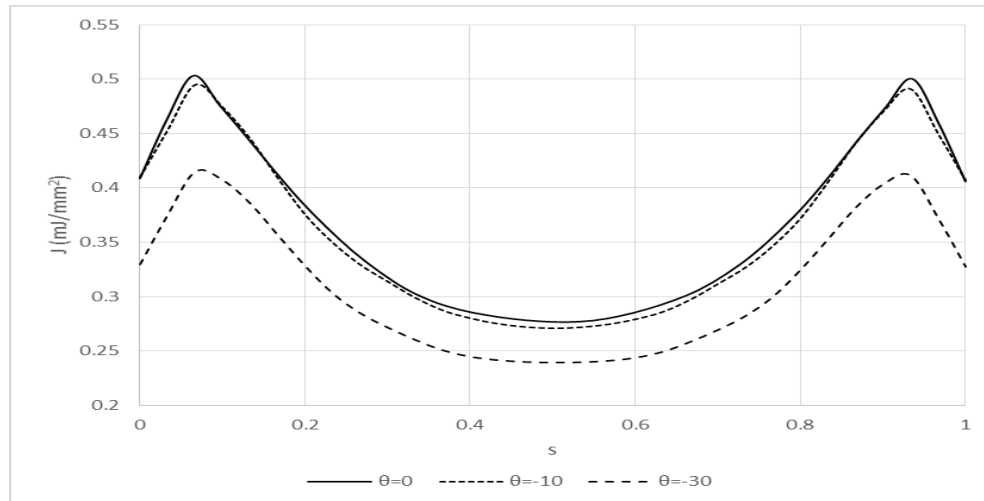


Figure 12. Variation of J plotted against s for a crack of a=b=1.651mm at a selected displacement load level of 0.037mm

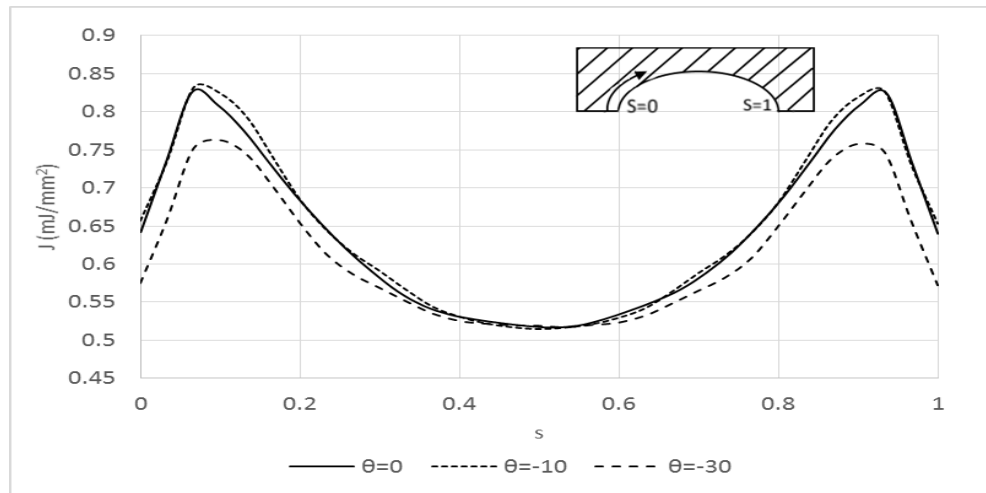


Figure 13. Variation of J plotted against s for a crack of $a=b=1.651\text{mm}$ at values of $\theta=0, -10$ and -30 with $J=0.53$ at s for all models

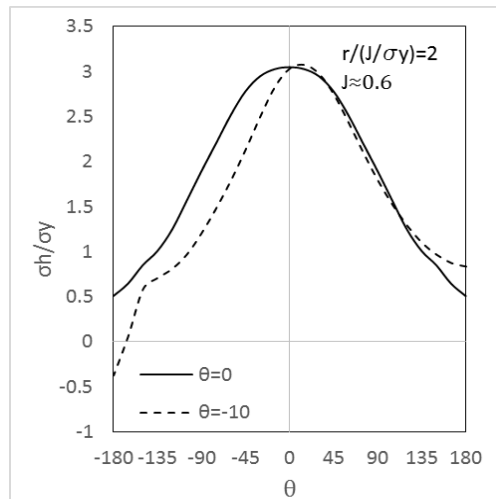


Figure 14. Hydrostatic stress versus θ for cracks of angles $\theta=0$ and $\theta=-10$

4. Conclusions

Based on a numerical study of the influence of flaw size and flaw orientation on response of a threaded fastener made from high strength steel, following are the key findings

1. Modifications to crack geometry were shown to have a significant influence on the value of the J -integral along the crack front. These results were also shown to have significant variation based on the load applied to the component.
2. Values of the J -integral were shown to reach a maximum in the vicinity of the free surface with minimal values occurring at the root of the crack.

3. A comparison of a crack perpendicular to the loading and a crack angle -10 degrees from the crack front show little variation in J . Despite this, a significant shift in the hydrostatic stress state seen ahead of the crack front when plotted against angular variation.
4. Increasing the crack angle to -30 degrees the J integral value sees a drastic change along the entire crack front. A plateau effect on the maximum J value along s is seen as the crack orientation angle is increased to -30 degrees, resulting in an overall drop in the magnitude of J .

REFERENCES

- [1] Rogers, D. "Fear of Failure: Why Bolts on London's Cheesegrater Tower Began to Break." GCR., 16 Jan. 2015.
- [2] Davidson, T. "An Introduction to Failure Analysis for Metallurgical Engineers." An Introduction to Failure Analysis for Metallurgical Engineers. The Minerals, and Materials Society, 1999.
- [3] Vorderbrueggen, L. "Bay Bridge Steel Bolt Failures Reveal Inadequate Metallurgy Expertise, Officials Say." San Jose Mercury News., 2013.
- [4] Tovey, Alan. "Cheesegrater Bolt Failures to Cost Severfield £6m." The Telegraph. Telegraph Media Group, 17 June 2015.
- [5] Schaub, Jeffery. "Millions To Be Spent Monitoring Bolts On New Bay Bridge." CBS San Francisco. CBS Local Media, 13 Jan. 2014.
- [6] "Container Lid Bolts for Low-level Nuclear Waste Might Be failing." Japan Times RSS., 28 June 2015.
- [7] Williams, M. L. "On the Stress Distribution at the Base of a Stationary Crack." Journal of Applied Mechanics 24 (1957): 109-14
- [8] Wells, A.A., "Unstable Crack Propagation in Metals: Cleavage and Fracture." Proceedings of the Crack Propagation Symposium, Vol. 1, (1961): Paper 84.
- [9] Rice, J. R. "A Path Independent Integral and the Approximate Analysis of Strain Concentration by Notches and Cracks." Journal of Applied Mechanics 35.2 (1968): 379-86.
- [10] Hutchinson, J.W. "Singular Behaviour at the End of a Tensile Crack in a Hardening Material." Journal of the Mechanics and Physics of Solids 16.1 (1968): 13-31.
- [11] Rice, J.R. "Limitations to the Small Scale Yielding Approximation for Crack Tip Plasticity." Journal of the Mechanics and Physics of Solids 22.1 (1974): 17-26.
- [12] Rice, J.R., and G.F. Rosengren. "Plane Strain Deformation near a Crack Tip in a Power-law Hardening Material." Journal of the Mechanics and Physics of Solids 16.1 (1968): 1-12.
- [13] Anderson, T. L. *Fracture Mechanics: Fundamentals and Applications*. Boca Raton, FL: Taylor & Francis, 2005.
- [14] Gao, X., Zhang, G., and Roe, C. "A Study on the Effect of the Stress State on Ductile Fracture." International Journal of Damage Mechanics 19.1 (2009): 75-94.
- [15] Gao, X., Zhang, T., Hayden, M., and Roe, C. "Effects of the Stress State on Plasticity and Ductile Failure of an Aluminum 5083 Alloy." International Journal of Plasticity 25.12 (2009): 2366-382.

- [16] *"DH36 Shipbuilding Steel Plate."* Shipbuilding Steel. Bebon International,
- [17] *SIMULIA* Abaqus. Program documentation. Vers. 6.13. Simulia, 2013.
- [18] *Hyperworks*. Vers. 13.0. Altair, 2014. Computer software.
- [19] *Inventor Professional*. Autodesk, 2014. Computer software.
- [20] Gao, X., and Dodds, R.H.Jr., *"Constraint Effects on the Ductile-to-brittle Transition Temperature of Ferritic Steels: A Weibull Stress Model."* International Journal of Fracture 102 (2000): 43-69.
- [21] Gao, Xiaosheng, and Robert H Dodds Jr. *"An Engineering Approach to Assess Constraint Effects on Cleavage Fracture Toughness."* Engineering Fracture Mechanics 68.3 (2001): 263-83.